Int j simul model 24 (2025) 1, 123-134
Original scientific paper

A SIMULATION-BASED OPTIMIZATION APPROACH TO ENHANCE DRIVE SHAFT FATIGUE STRENGTH

Yang, L.[*]; Wang, L. Y.[**,#]; Li, L.[**]; Zheng, X. H.[***] & Chang, S. Y.[*]

[*] Key Laboratory of Advanced Manufacturing Technology, Beijing University of Technology, Beijing, 100124, China

[**] The Ministry of Education, Key Laboratory of Modern Measurement and Control Technology, Beijing Information Science &Technology University, Beijing, 100192, China

[***] China Geological Survey, China Aero Geophysical Survey & Remote Sensing Center, Beijing, 100083, China

E-Mail: wly_bistu@126.com ([#] Corresponding author)

Abstract

This study presents a novel simulation-based optimization approach to enhance drive shaft fatigue strength using Bayesian-Kriging surrogate model. The methodology incorporates three key innovations: (1) a Python-based parametric model development using ABAQUS, (2) an entropy weight TOPSIS method for dimensional contribution analysis, and (3) a Bayesian Expected Improvement (BYEI) strategy for enhanced Kriging model performance. The proposed method significantly reduces computational cost while maintaining accuracy through intelligent sampling and model updating strategies. Validation using three test functions demonstrates superior convergence speed, stability, and accuracy compared to traditional methods. Application to drive shaft optimization achieved a 56.11 % improvement in fatigue life while maintaining structural constraints. Compared with the other two models, Bayesian-Kriging model has obvious advantages in prediction accuracy. The results demonstrate the method's effectiveness for complex mechanical component optimization, particularly in scenarios requiring balance between computational efficiency and accuracy.

(Received in August 2024, accepted in November 2024. This paper was with the authors 1 month for 1 revision.)

Key Words: Entropy Weight TOPSIS, Kriging, Simulation, Optimization Design

1. INTRODUCTION

The performance of the drive shaft in special vehicles impacts the functionality and reliability of the entire vehicle system, with torsional fatigue being the primary mode of failure [1]. However, the complexity of the finite element analysis (FEA) process for the drive shaft poses a challenge in fatigue strength optimization design. Conducting a structural finite element static analysis is time-consuming, and fatigue strength optimization methods necessitates a large sample size for structural analysis, often requiring numerous iterative calculations to determine the optimal solution [2, 3]. Consequently, there is a critical need to propose an efficient fatigue strength optimization method that significantly reduces the calculation time while ensuring accuracy.

At present, fatigue strength optimization methods are mostly developed based on finite element topology optimization method, which necessitates reliance on existing design experience for conducting iterative simulation experiments and model adjustments. This approach is characterized by prolonged modelling duration, low optimization efficiency, unclear topology boundaries, and complex sensitivity calculations during the optimization process, leading to limitations in universality and reliability [4]. In recent years, scholars have increasingly employed surrogate models such as radial basis function, support vector machine and Kriging to approximate complex and high-precision numerical simulation models to fit complex and high-precision numerical simulation models, and constructed approximate objective functions or constraint functions to characterize the performance response of

structures. Intelligent algorithms are used to optimize and solve them, thereby reducing the computational cost and time of lightweight design [5-7].

The existing fatigue strength optimization methods based on surrogate model are difficult to meet the actual needs of engineering in terms of accuracy, efficiency and generalization ability [8, 9]. This study proposes a simulation optimization method for fatigue strength of drive shaft based on Bayesian-Kriging surrogate model. A parametric model of the drive shaft is developed using Python's ABAQUS secondary development, enabling a rapid and efficient analysis of stress and strain responses in the current drive shaft model under typical operating conditions. To reduce the dimension of optimization problem, the Entropy-weighted Technique for Order Preference by Similarity to Ideal Solution (TOPSIS) method is used to calculate the contribution of key structural parameters to the output response of the transmission shaft. A Control Function (CF) is established by using Bayesian posterior characteristics, and a Kriging surrogate model of Bayesian Expectation Improved control (BYEI) is established to improve the fatigue strength of the drive shaft by introducing the classical expectation adding point strategy.

2. MODELLING AND FEA OF DRIVE SHAFT

2.1 Parametric geometry modelling

This study establishes the coordinate parameter equation for involute and spiral line series points based on mechanical design principles and mathematical analysis methods. Additionally, a novel method for accurately modelling spur involute splines is proposed using Python's ABAQUS secondary development capabilities. This method enables the precise and convenient establishment of spur involute spline models. Python script is executed to generate the involute outer spline in ABAQUS (Fig. 1 a). The coordinates of the continuous points on the involute are determined based on the involute curve equation, and the involute is constructed through continuous point fitting.

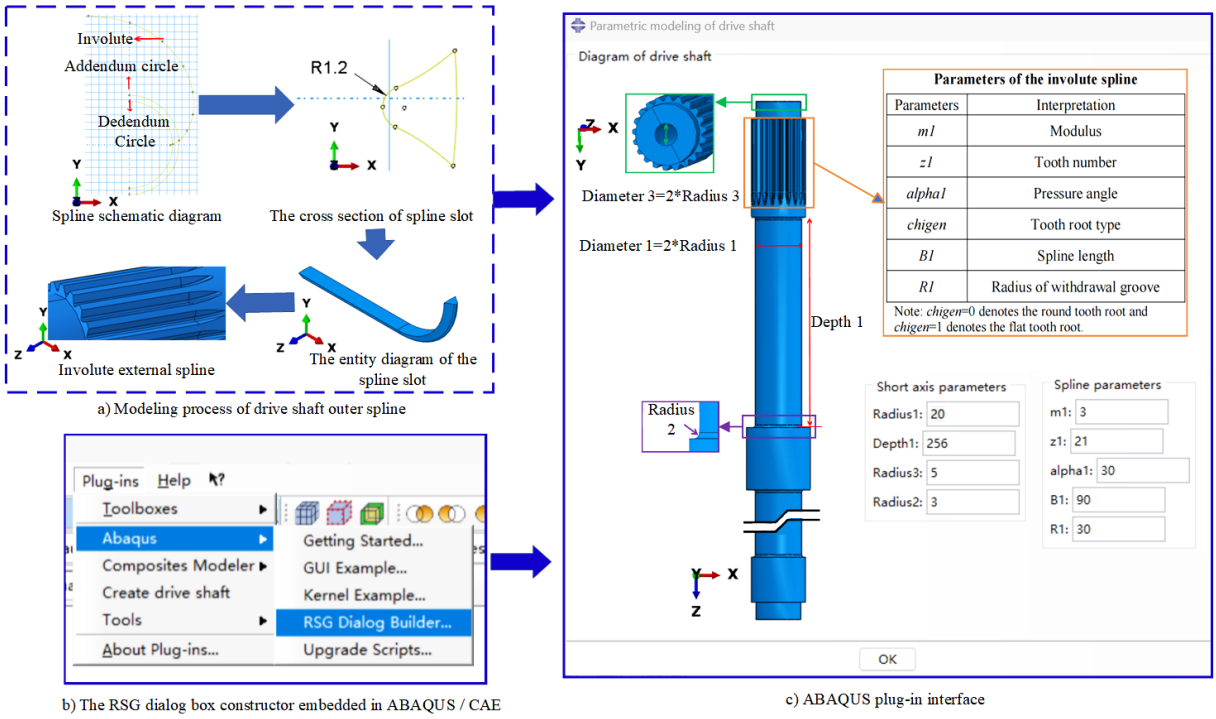

Figure 1: Drive shaft modelling plug-in.

The keyway entity corresponding to the involute outer spline is created through sweeping and stretching. Finally, the involute outer spline is generated by utilizing the functionality of the assembly module to eliminate the entity. Additionally, in the shaft section parameters, the outer diameter, inner diameter, and transition fillet of the short shaft end are essential geometric factors that determine the operational stress of the drive shaft [10]. The RSG dialog box constructor embedded in ABAQUS / CAE is shown in Fig. 1 b, which is an auxiliary tool for GUI plug-in development [11]. This study uses this tool to create a simple drive shaft modelling plug-in interface as shown in Fig. 1 c. The Python script is used as the kernel file executed by the plug-in to complete the rapid modelling of the drive shaft. This approach not only establishes the model foundation for subsequent EFA but also significantly enhances the accuracy and efficiency of fatigue strength optimization design for the drive shaft.

2.2 FEA

According to the test and real vehicle observation results, cracks consistently develop at the tooth root of the spline located at the short shaft end. To expedite calculations, the intermediate spline and the long shaft end are simplified as the optical axis, rendering the drive shaft an axisymmetric model. The short shaft end of the drive shaft features 21 splines. Leveraging ABAQUS's cyclic symmetric interaction capability, a model representing 1/21 of the entire spline structure is constructed. The model comprises a total of 60,203 elements, with element type C3D10.

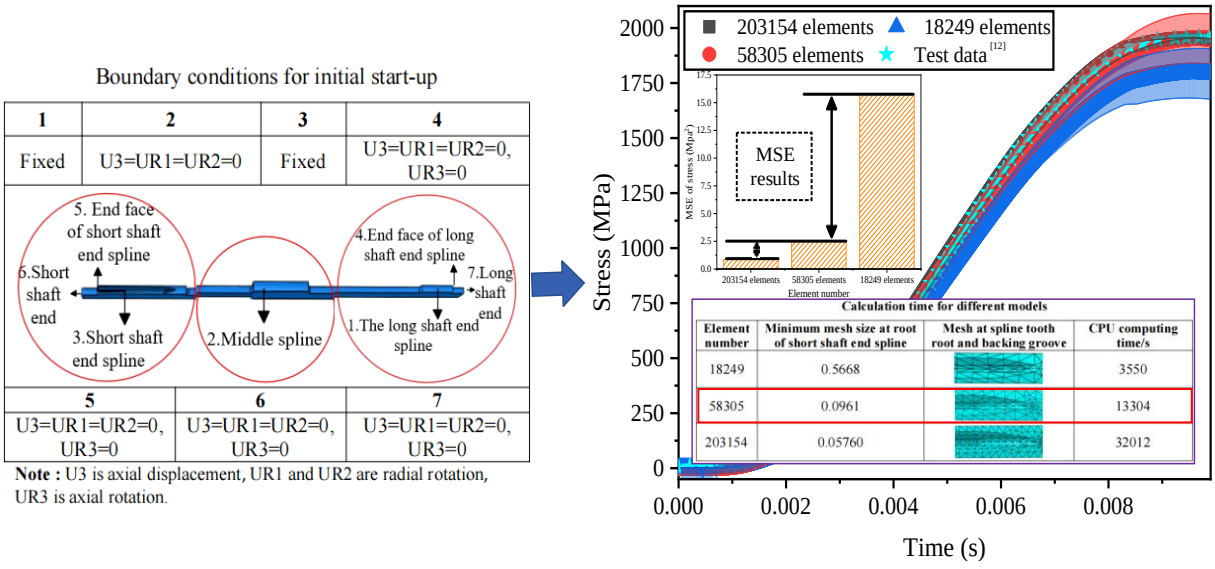

Figure 2: Stress change curves for different models.

The material's elastic modulus is 210 GPa, and the Poisson's ratio is 0.3. Boundary conditions is detailed in Fig. 2. A torque of 9815.12 Nm (corresponding to the maximum output power) is applied to the middle spline, while the splines at both ends are fixed (tooth surface displacement constraint). This setup represents a typical starting condition and the most precarious limit condition for the short shaft end. The study begins with a convergence analysis aimed at determining the optimal mesh size for the element model. Fig. 2 illustrates the time history of the maximum stress point. The material parameters of this study were derived from the literature [12], and the test data were also derived from this literature. Because the output interval of the calculation results is small and the data points are dense, the error bar is banded in Fig. 2. By further calculating the Mean Squared Error (*MSE*) of the three models, it reveals that beyond 58305 grids, the stress results exhibit minimal variation, and the computational

time remains within an acceptable range. Consequently, the model is partitioned into 58305 grids, with the smallest grid size at the tooth root of the short shaft end spline measuring 0.0961.

FEA of the initial simplified model of the drive shaft was conducted, and the stress distribution cloud map and deformation cloud map results were obtained (Figs. 3 a and 3 b). After conducting a comparative analysis, it was found that the maximum Mises stress at the optical axis of the short shaft end is 2.8 times higher than the maximum Mises stress at the optical axis of the long shaft end [12]. This value is approximately equivalent to the torsional stiffness ratio on both sides of the transmission shaft. The maximum Mises stress of the transmission spindle is located at the short shaft end, measuring 1694 MPa. The presence of local stress concentration, attributed to geometric mutation, leads to the highest stress levels at the root part of the junction between the short shaft spline and the retreating groove. The transmission shaft exhibits geometric mutation and an uneven structure, contributing to local stress concentration and resulting in local yield at the root of the notch, forming a plastic zone. Under a short-time impact load, microplastic deformation and micro-cracks may occur. The area of actual crack generation identified through bench testing is depicted in Fig. 3 c. The location of maximum stress aligns with the actual fatigue fracture position of the transmission spindle, thereby confirming the accuracy of FEA. High cycle fatigue-induced strain damage is likely to initiate crack formation at the notch.

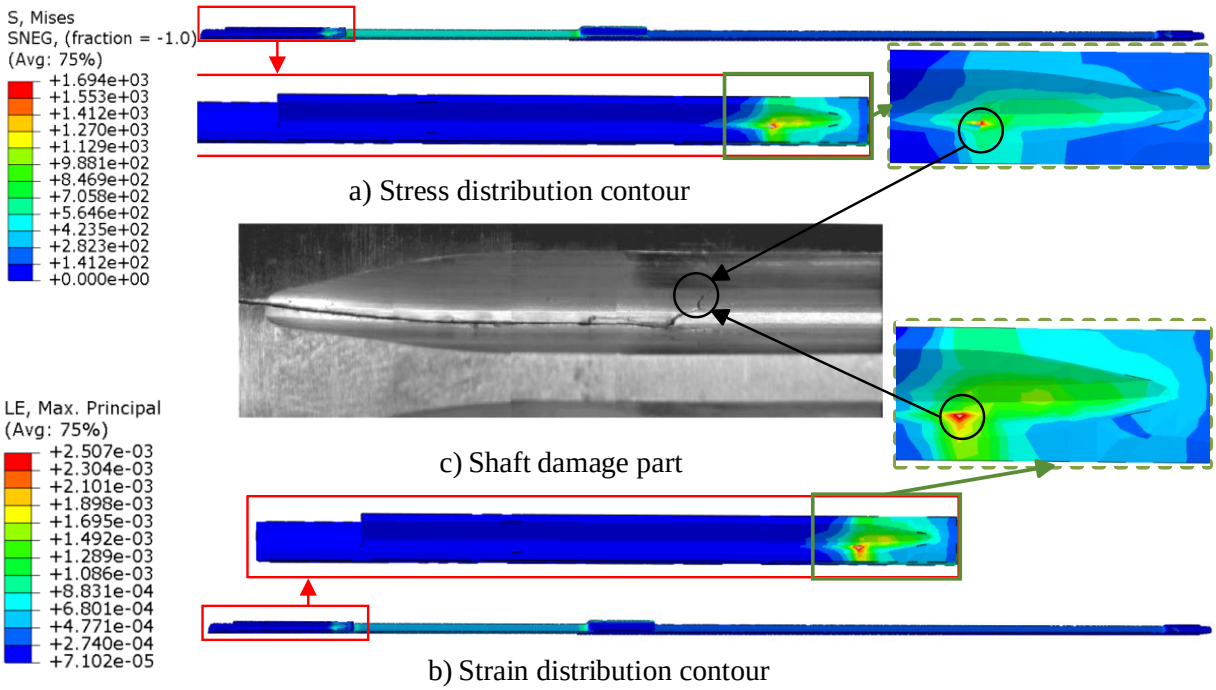

Figure 3: Stress and strain distribution.

2.3 Contribution analysis

For general parameter optimization issues, the efficiency and accuracy of optimization decrease as the dimension of design variables increases. To address this challenge, this study employs the entropy weight TOPSIS method to identify the two design variables that exert the most significant impact on the performance response of the drive shaft. This approach allows for a more intuitive analysis of the impact of each design variable on the drive shaft's performance response. Furthermore, it has the potential to enhance the efficiency and accuracy of subsequent optimization designs for drive shaft fatigue strength simulations. To analyse the individual contributions of these design variables, an orthogonal experimental design was employed. Each design variable was adjusted by ±2 mm from its initial value, resulting in a 4-level design

L16(44). FEA was then used to evaluate the impact of these design variables on key performance metrics of the drive shaft, including *M*, *F*, *S*, *U*, and *N*. Technique for TOPSIS method was utilized to calculate the individual contributions of the aforementioned design variables to each response index (Fig. 4).

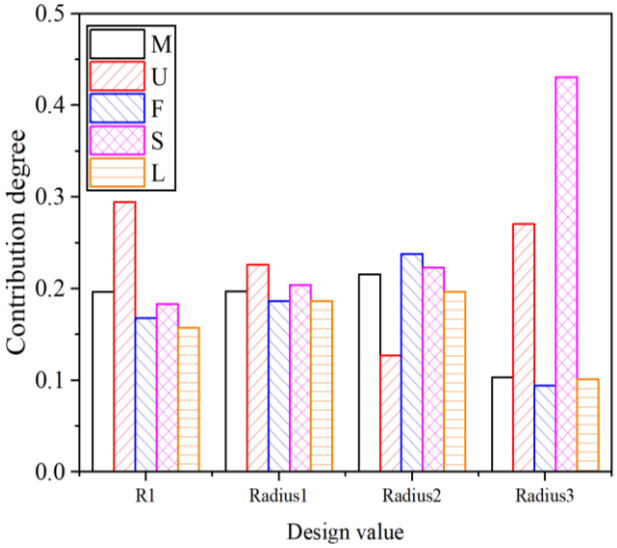

Figure 4: Single contribution of each design variable to response index.

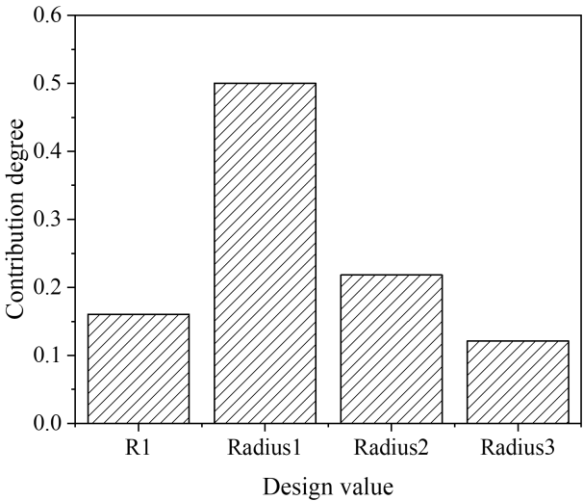

Figure 5: Comprehensive contribution of design variables to response index.

Radius1 and *Radius2* significantly impact *M*, *F*, and *N* of the system. Furthermore, *Radius2* has an impact on *S*. *Radius3* plays a crucial role in *U* and S, while *R1* primarily impacts *U*. Here, *R1* refers to the radius of the relief groove, and *Radius1* refers to the radius of the short axis, as shown in Fig. 1. *M* and *N* are more crucial compared to the other three response indicators. To address this, the entropy weight TOPSIS method is employed for calculating the comprehensive contribution of design variables based on single contribution calculation as shown in Fig. 5. The analysis indicates that *Radius1* and *Radius2* exhibit the most significant comprehensive contributions to all the aforementioned response indicators. Consequently, these two design variables have been identified as the key parameters for the fatigue strength optimization design of the drive shaft.

3. SIMULATION OPTIMIZATION DESIGN METHOD

This paper proposes a simulation and optimization design method for enhancing the fatigue strength of the drive shaft, utilizing an improved Kriging surrogate model in conjunction with a genetic algorithm. Fig. 6 illustrates the flow chart for the fatigue strength optimization design of the drive shaft. Design variables with high comprehensive contribution determined by the entropy weight TOPSIS method are selected as input parameters, with mass and performance responses from FEA serving as constraints. The optimal Latin hypercube sampling method is used to extract the initial sample points, and the response value is obtained by EFA. *N* results are utilized as optimization objectives to formulate a mathematical model. A mathematical model for fatigue strength optimization is established.

An improved Kriging surrogate model is then established and verified. Kriging model demonstrates high efficiency in modelling with limited samples, making it well suited for surrogate optimization in various optimization problems. When the average relative error *ERR* of the prediction points meets the accuracy requirements, the point addition strategy is required to update the Kriging model. Expected Improvement (EI) strategy plays a pivotal role in model management and sample updating. However, a drawback of EI selection strategy is its tendency

to be greedy, potentially causing new sample points to cluster around local extrema [13]. To address these issues, as shown in the introduction of algorithm theory in Fig. 6, BYEI point addition strategy is proposed by integrating a Control Function (CF) into EI strategy. The CF is designed to dynamically adjust the placement of new test points to enable efficient and accurate approximations, thereby enhancing the balance between global and local exploration capabilities for more effective point additions. Building upon this framework, Kriging surrogate model is iteratively updated, culminating in the establishment of Kriging surrogate model with BYEI. Although the introduction of CF in the EI strategy can enhance the global search ability of the random term $Z(x)$ of the Kriging algorithm, it does not improve the prediction accuracy of the model regression term $\Sigma b_i f_i(x)$. In the future, the PCE model can be considered to replace the regression term d to establish a hybrid surrogate model. On this basis, the BYEI strategy can be used to further improve the ability of the Kriging model to solve optimization problems.

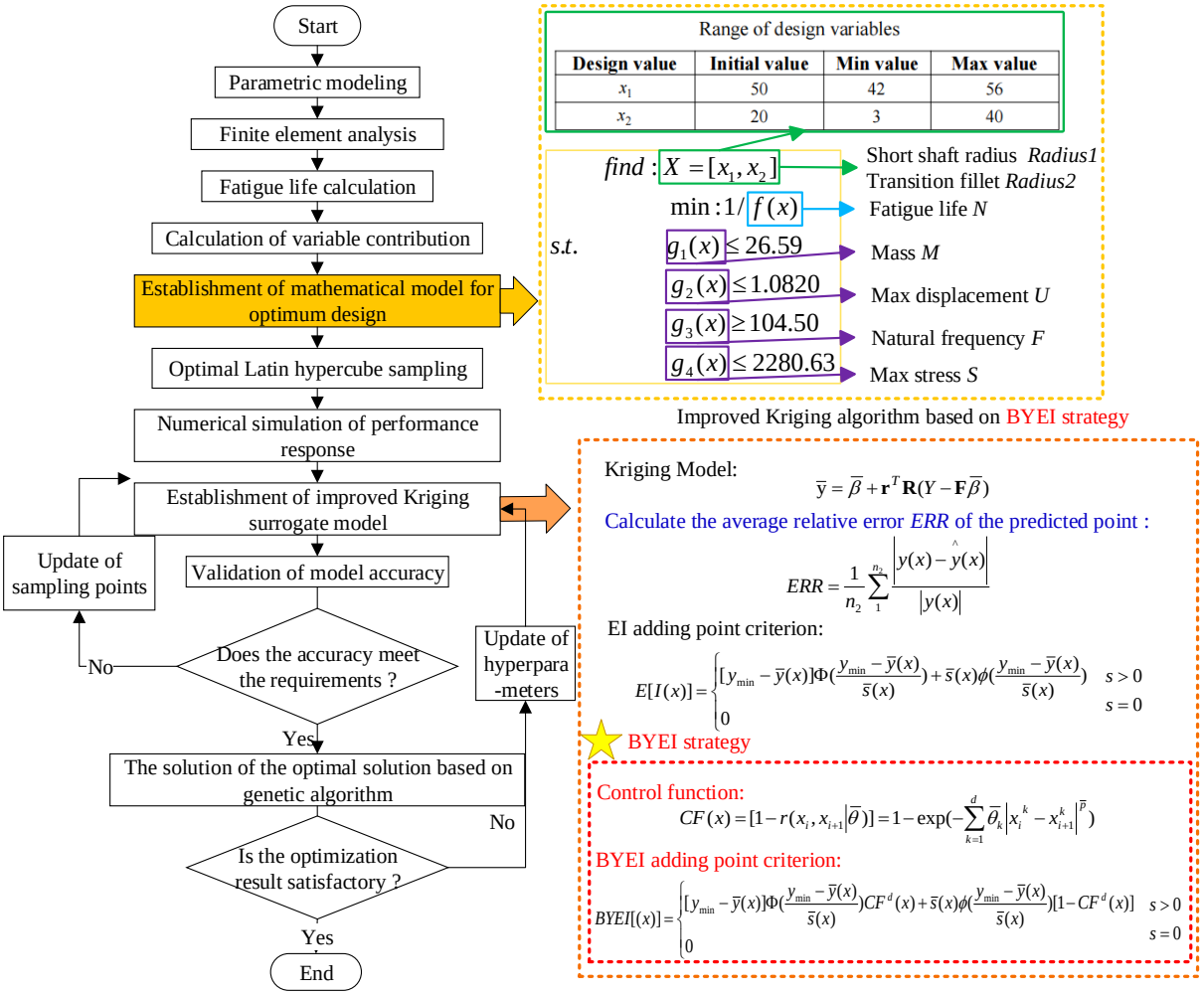

Figure 6: Fatigue strength simulation and optimization design platform for drive shaft.

4. RESULTS AND DISCUSSIONS

Three unconstrained test functions were chosen to assess the effectiveness of Kriging surrogate model using the proposed BYEI point addition strategy. The evaluation focused on three key aspects: iteration count, model accuracy, and robustness. Subsequently, the optimization results of Kriging surrogate model with BYEI addition strategy were examined. Initially, the precision of the response value fitting was evaluated, followed by a discussion on the optimization performance of the model.

4.1 Analysis of the superiority of the optimization model

To demonstrate the effectiveness of BYEI addition strategy, three test functions (Squared, Branin, and Paulson) were utilized to compare and evaluate the optimization performance of various algorithms based on three criteria: iteration count, model accuracy, and robustness. The convergence rate of SBO method is primarily assessed by the number of iterations required for the approximate response value to converge near the known optimal response value. A faster convergence rate is indicated by a lower number of iterations. To illustrate the optimization impact of BYEI strategy, EI, WEI single-point filling strategy, and adding point filling strategy were chosen for 30 optimization repetitions each. Subsequently, the convergence curve of the average optimal response from the 30 optimization runs was plotted against the number of iterations.

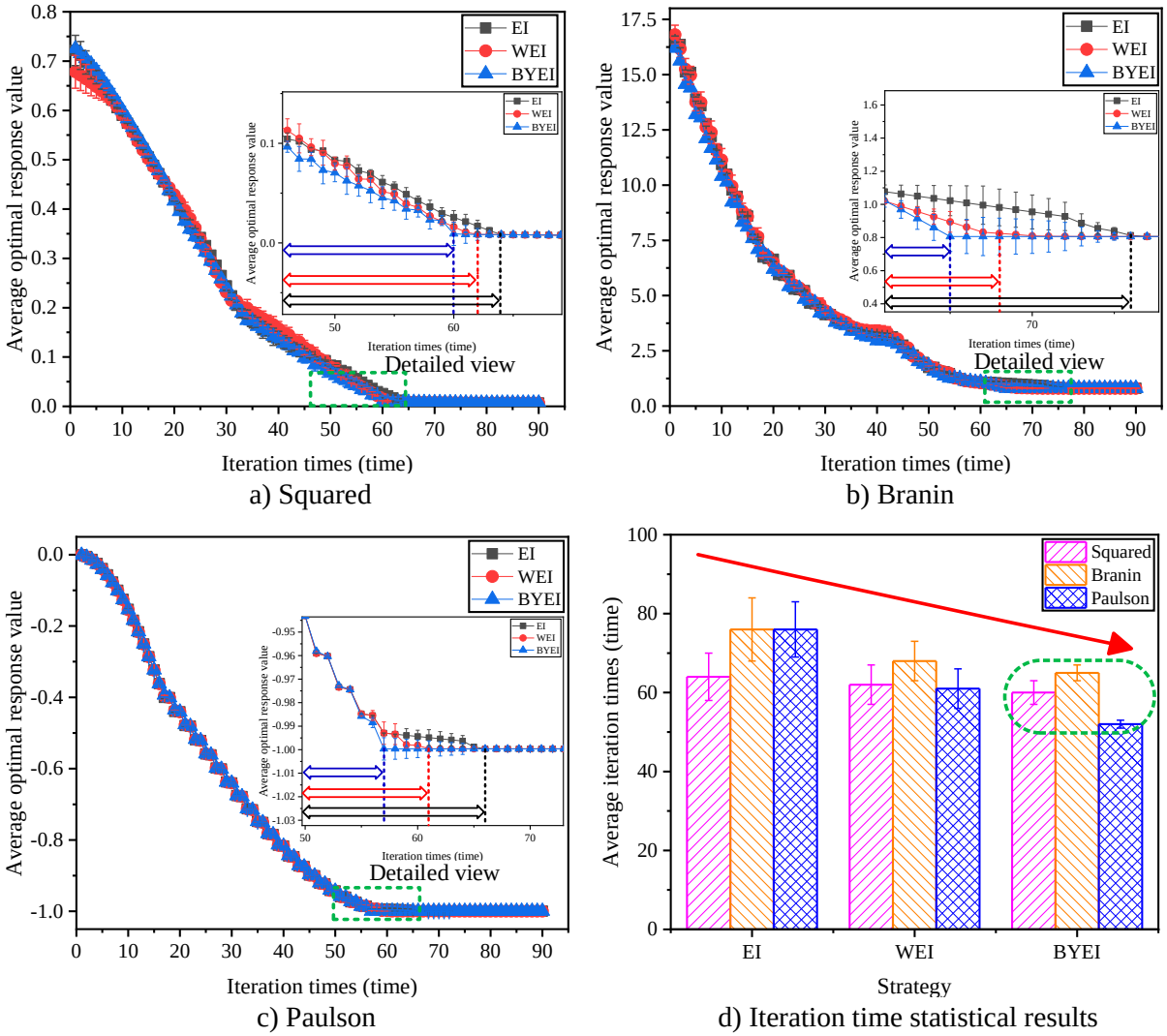

Figure 7: Comparison of optimization results using EI, WEI, and BYEI algorithms for different test functions.

In Figs. 7 a to 7 c, with an increase in the number of iterations, all strategies demonstrate convergence towards the optimal response value, suggesting the effectiveness of the three optimization methods. Combined with the statistical results of Fig. 7 d, analysis of the convergence speed of the approximate optimal response reveals that BYEI method outperforms EI and WEI methods. This indicates that BYEI strategy can significantly enhance computational efficiency and lower testing costs.

To explore the resilience of the proposed optimization approach, thirty sets of random experiments were conducted on EI, WEI, and BYEI strategies across three test functions. The results were used to generate a box plot illustrating the approximate optimal response values (Figs. 8 a to 8 c). A flatter box plot with fewer outliers indicates better robustness. The analysis reveals that, in all three scenarios, the WEI method produces a box plot with fewer outliers and a flatter distribution compared to the parameter optimization methods employed in EI and WEI strategies. Furthermore, BYEI strategy demonstrates superior performance with almost no outliers and a flatter box plot when contrasted with the traditional EI and WEI strategies. The statistical results of Fig. 8 d show that the parameter optimization method associated with BYEI strategy exhibits greater robustness.

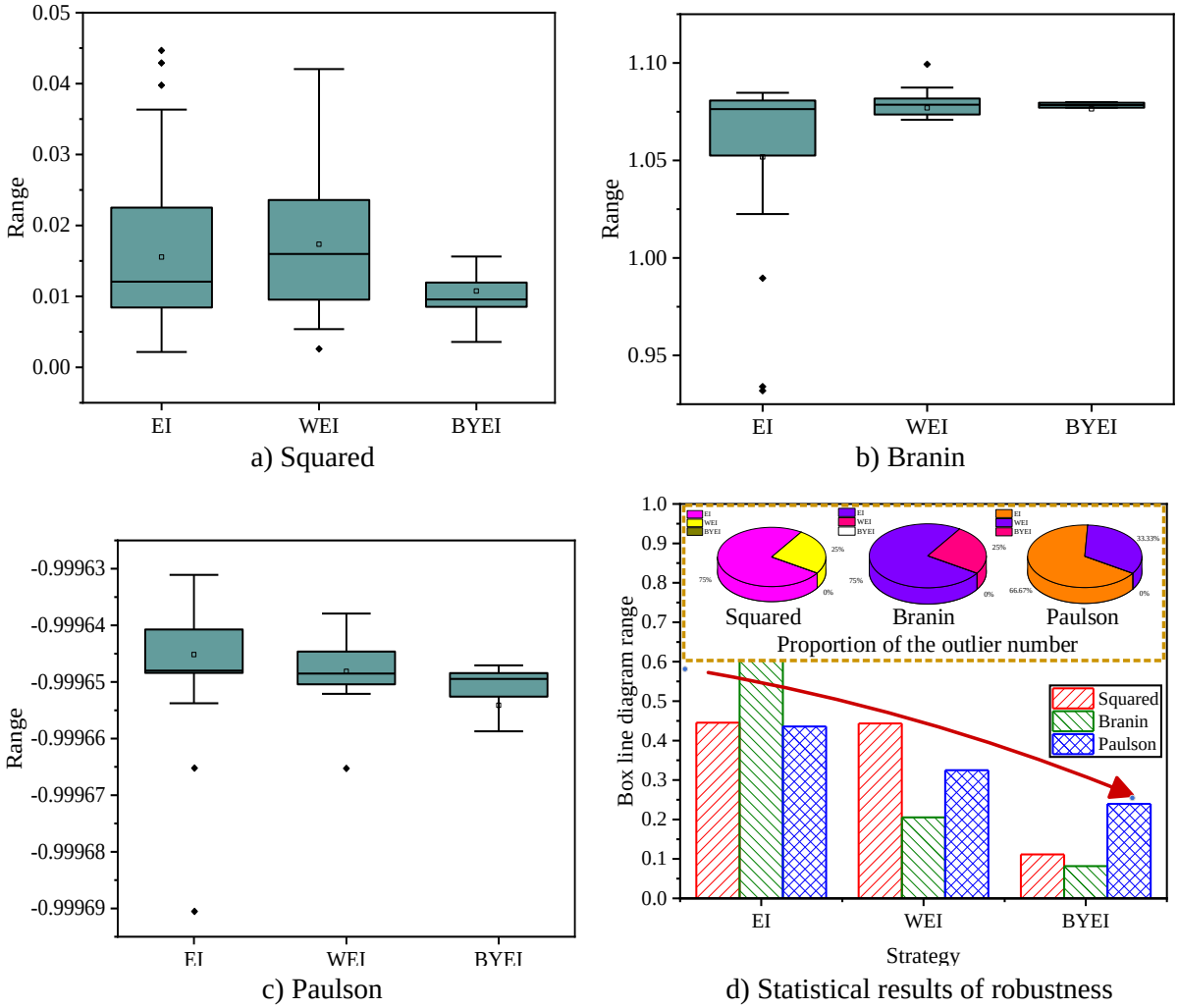

Figure 8: Final optimization results comparison using different strategies for test examples.

Root mean square error r_1 and mean absolute percent error r_2 were chosen as the metrics to evaluate the prediction accuracy of the model. The equations for r_1 and r_2 are presented as follows, a lower value indicates a higher level of prediction accuracy for the model:

$$r_1 = \sqrt{\frac{1}{N}\sum_{i=1}^{N}(\bar{y}_i - y_i)^2} \qquad (1), \qquad r_2 = \frac{1}{N}\sum_{i=1}^{N}\left|\frac{\bar{y}_i - y_i}{\bar{y}_i}\right| \times 100\% \qquad (2)$$

where $\bar{y}_i$ and y_i are the real response values and the predicted response values of Kriging model, N is the number of model predictions.

Table I: r_1 and r_2 mean of 30 repeated trials with different optimization methods.

Strategy	r_1			r_2		
	Squared	**Branin**	**Paulson**	**Squared**	**Branin**	**Paulson**
EI-Kriging	0.003674	0.009108	0.009004	5.0982 %	6.7660 %	6.4604 %
WEI-Kriging	0.003976	0.008465	0.008336	4.8820 %	6.2916 %	5.4088 %
BYEI-Kriging	0.001225	0.002841	0.003918	0.4506 %	0.4135 %	0.8716 %
PCE [13]	0.003884	0.009548	0.009564	6.0489 %	6.1484 %	7.0981 %
SVR [13]	0.004031	0.009487	0.009168	4.9889 %	6.948l %	6.9988 %
Statistical results of calculation accuracy						
Strategy	r_1			r_2		
	Average value	**Standard deviation**		**Average value**	**Standard deviation**	
EI-Kriging	0.007262	0.003107		6.1082 %	0.8879 %	
WEI-Kriging	0.006926	0.002555		5.5274 %	0.7122 %	
BYEI-Kriging	0.002661	0.001355		0.5785 %	0.2544 %	
PCE [13]	0.007665	0.003274		6.4318 %	0.5791 %	
SVR [13]	0.007562	0.003062		5.99385 %	1.4212 %	

In the three scenarios (Table I), r_1 values of EI, WEI, and BYEI after 30 iterations are all below 0.01, with r_2 values being less than 0.1. The precision of Kriging model under the three control strategies fulfils the criteria. The accuracy levels of EI and WEI approaches exhibit minimal disparity, whereas r_1 and r_2 values of BYEI approach are notably lower than those of the former two methods, suggesting that BYEI strategy offers superior calculation accuracy. Support Vector Regression (SVR) model and Polynomial Chaos Expansion (PCE) model are often used to compare with Kriging model [13]. The iteration speed and robustness depend on specific analysis problems and parameter search methods, and the comparison results are not representative. Therefore, we focus on the prediction accuracy of test function values. It can be seen from Table I that the prediction results of the PCE model and the SVR model are close to the Kriging model under the EI strategy, and the Kriging model under the BYEI strategy has obvious advantages in prediction accuracy.

4.2 Analysis of the results of the optimization model

The study employs optimal Latin hypercube sampling to generate 20 sets of samples. These samples are used to fit *M*, *F*, *S*, *U*, and *N* using a Kriging model guided by BYEI optimization strategy. The optimization problem is then solved using a genetic algorithm. The error scatter plot for each response variable is depicted in Fig. 9. The distribution of error points along the 45° diagonal suggests that Kriging model, under the control of BYEI optimization strategy, exhibits a strong fitting performance.

The optimization results of the surrogate model managed by BYEI addition point optimization strategy are presented in Table II. The computational results indicate that *M*, *F*, *U*, and *S* at the optimal solution of each surrogate model fall within the specified constraint boundaries. In comparison to the model utilizing the initial design variable values, the optimized model exhibits increased *M* and *F*, while experiencing decreased local *S* and *U*, leading to an enhanced final *N*. The optimization approach implemented results in a 2.35 % enhancement in the drive shaft *M*, a 3.98 % increase in *F*, a 21.33 % reduction in local *S*, and a 4.12 % decrease in *U*. Consequently, the average *N* of the drive shaft structure rises from 7,818 cycles to 12,204 cycles, marking a 56.11 % improvement. The structure of the drive shaft before and after optimization is illustrated in Figs. 11 a and 11 b, respectively. *Radius1* has been marginally enlarged, whereas the dimensions of the transitional fillet have been significantly diminished.

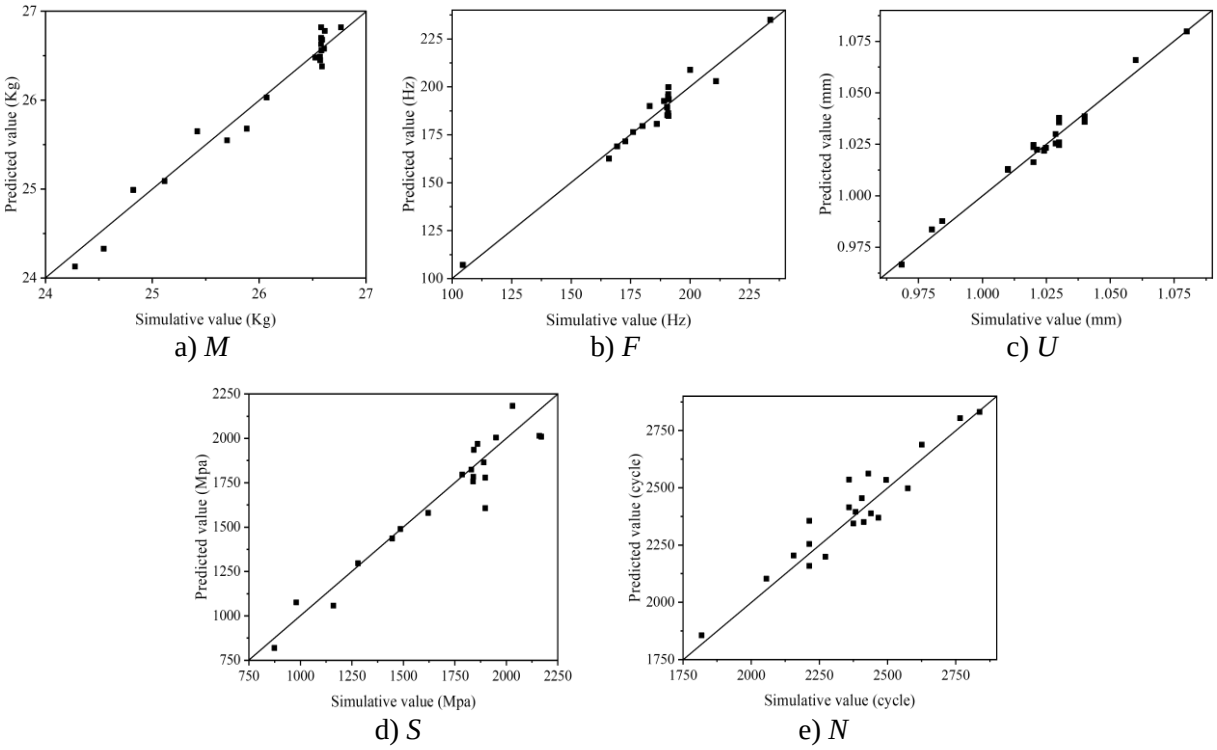

Figure 9: Kriging model error scatter plot of BYEI optimization strategy control.

Table II: Optimization results of Kriging surrogate model using BYEI point addition strategy.

Name	**Initial values**	**Value range**	**Optimal values**	**Change ratio** /%
Design variable value (x_1, x_2) /mm	(50.00, 20.00)	(42~56, 3~40)	(52.14, 3)	/
M /kg	25.11	0~26.59	25.71	2.35
F /Hz	176.31	0~104.50	183.10	3.98
S /Mpa	1548.32	0~2280.63	1276.11	-21.33
U /mm	1.0131	0~1.0820	0.9684	-4.12
N /cycle	7818	-	12204	56.11

The strain distribution is also depicted in Figs. 10 a and 10 b. *N* of the drive shaft is predominantly impacted by the strain concentration at the spline of the short shaft end, as determined by TOPSIS entropy weight method. Therefore, the primary optimization procedure involves modifying the dimensions of the short shaft end shaft to alleviate strain concentration and minimize the maximum local deformation at the spline. Therefore, the primary objective of optimization is to modify the dimensions of the short shaft to alleviate strain concentration and minimize the maximum local deformation at the spline. A comparison of the drive shaft's shape before and after optimization reveals strain concentration at the spline tooth root in both cases. However, enhancing *Radius1* and decreasing *Radius2* results in an improved strain distribution along the drive shaft post-optimization compared to its pre-optimized state.

This study not only effectively improves the fatigue strength of the drive shaft by changing the key structural dimensions, but also provides an economical and efficient optimization design method for other industrial products. However, the BYEI addition strategy in this study only improves the prediction accuracy of the random term of the Kriging model, and has no obvious effect on its regression term. In the future research work, we consider using the PCE model to replace the regression term to establish a hybrid agent model, and consider optimizing the BYEI strategy to establish a self-learning / adaptive hybrid agent model.

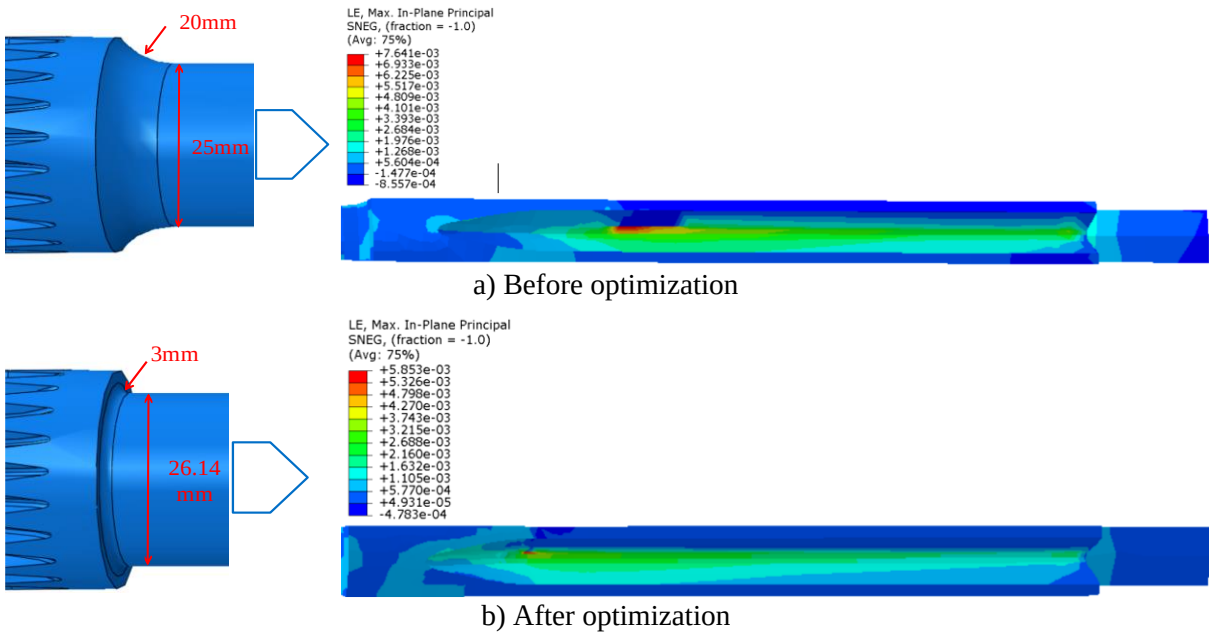

Figure 10: Drive shaft structure and strain distribution in withdrawal groove.

5. CONCLUSION

Current research on the structural fatigue strength optimization design heavily relies on FEA, which is characterized by high computational costs and low optimization efficiency. To address this issue, this paper proposes a novel fatigue strength optimization method for drive shafts based on an improved Kriging surrogate model. The approach begins with an analysis of the comprehensive contribution of structural size by combining the parametric model of the drive shaft with the entropy weight TOPSIS method. An improved Kriging surrogate model is then established using BYEI. This improved surrogate model is utilized to optimize the structural size with the highest contribution, ultimately aiming to enhance *N* of the drive shaft. The following conclusions are drawn from this study:

1. FEA results indicate that selecting a 30° tooth root spline significantly improves the structural strength and service life of the spline. The entropy weight TOPSIS method identifies that *Radius1* and *Radius2* of the drive shaft contribute the most comprehensively to all response indicators.
2. Comparing the results of three function examples, Kriging surrogate model under the proposed improved control strategy demonstrates faster iteration speed, stronger robustness, and higher calculation accuracy.
3. By employing Kriging model with the improved control strategy for optimizing the fatigue strength of the drive shaft, *N* of the drive shaft is increased by 56.11 %. This optimization is achieved while minimizing *M*, *U*, and *S*, and simultaneously increasing *F*.

ACKNOWLEDGEMENT

The research described in this paper was financially supported by the National Natural Science Foundation of China (52175074).

REFERENCES

[1] Milkovic, M.; Njegovec, M.; Predan, J.; Javornik, J.; Djonlagic, D.; Gubeljak, N. (2023). Monitoring surface state of AA7075-T6 during dynamic loading with FBG sensor, *International Journal of Simulation Modelling*, Vol. 22, No. 4, 631-642, doi:10.2507/IJSIMM22-4-663

[2] Liu, J. D.; Chen, J. Q.; Wu, J. Q.; Han, F.; Guan, J. F. (2023). Simulation method for stitch wire vibration load and fatigue life, *International Journal of Simulation Modelling*, Vol. 22, No. 4, 643-654, doi:10.2507/IJSIMM22-4-664

[3] Rehman, T. U.; Li, J.; Qaiser, Z.; Johnson, S. (2024). A design framework for semi-active structural controlled adjustable constant force mechanisms, *Journal of Mechanical Design*, Vol. 146, No. 7, Paper 073301, 8 pages, doi:10.1115/1.4064248

[4] Li, J.; Rehman, T. U.; Qaiser, Z.; Johnson, S. (2024). Design optimization and validation of compliant bidirectional constant force mechanisms, *Mechanism and Machine Theory*, Vol. 195, Paper 105593, 14 pages, doi:10.1016/j.mechmachtheory.2024.105593

[5] Wang, H. J.; Yu, C. W.; Zhu, X. S.; Jian, L.; Lu, C. C.; Pan, X. G. (2024). Elevator block brake structural optimization design based on an approximate model, *PLoS ONE*, Vol. 19, No. 3, Paper e0296753, 22 pages, doi:10.1371/journal.pone.0296753

[6] He, C. L.; Zhang, Y.; Gong, D. W.; Ji, X. F. (2023). A review of surrogate-assisted evolutionary algorithms for expensive optimization problems, *Expert Systems with Applications*, Vol. 217, Paper 119495, 13 pages, doi:10.1016/j.eswa.2022.119495

[7] Mou, C. H.; Smith, L. M.; Chen, N. (2023). Combining stochastic parameterized reduced-order models with machine learning for data assimilation and uncertainty quantification with partial observations, *Journal of Advances in Modeling Earth Systems*, Vol. 15, No. 10, Paper e2022MS003597, 28 pages, doi:10.1029/2022MS003597

[8] Wang, B. C.; Liu, C. Z.; Zhang, L. T.; Wang, D. S. (2022). An innovative multi-sensor data fusion method based on thrice deeply-fusion architecture for multi-object tracking, *Proceedings of the Institution of Mechanical Engineers, Part D: Journal of Automobile Engineering*, Vol. 237, No. 12, 2679-2695, doi:10.1177/09544070221133151

[9] Brown, J. L.; Davis, J.-P.; Tucker, J. D.; Huerta, G.; Shuler, K. W. (2023). Quantifying uncertainty in analysis of shockless dynamic compression experiments on platinum. II. Bayesian model calibration, *Journal of Applied Physics*, Vol. 134, No. 23, Paper 235902, 21 pages, doi:10.1063/5.0173652

[10] Rasovic, N.; Cekic, A.; Kaljun, J. (2022). Design and simulation of the controlled failure of custom-built rigid shaft coupling, *International Journal of Simulation Modelling*, Vol. 21, No. 3, 383-394, doi:10.2507/IJSIMM21-3-596

[11] Zheng, M. P.; Li, Y. F.; Wang, C.; Bai, J. F.; Wang, L. H.; Liu, Z. F.; Wahab, M. A. (2023). Prediction of contact stress in bolted joints using the Polynomial Chaos-Kriging model, *Engineering Failure Analysis*, Vol. 154, Paper 107646, 19 pages, doi:10.1016/j.engfailanal.2023.107646

[12] Mohamed, H. S.; Elsawah, A. M.; Shao, Y. B.; Wu, C. S.; Bakri, M. (2023). Analysis on the shear failure of HSS S690-CWGs via mathematical modelling, *Engineering Failure Analysis*, Vol. 143, Part A, Paper 106881, 23 pages, doi:10.1016/j.engfailanal.2022.106881

[13] Liu, A. Y.; Yue, D. Z.; Chen, J. L.; Chen, H. (2024). Deep learning for intelligent production scheduling optimization, *International Journal of Simulation Modelling*, Vol. 23, No. 1, 172-183, doi:10.2507/IJSIMM23-1-CO4